We made elliptical isophote fits to the galaxy surface-brightness profiles, which allows us to determine unbiased scale-lengths at 0.2-arcsec resolution (FWHM)[15,18,21]. Spectra obtained with the Multiple Mirror telescope (MMT) were used to measure redshifts out to $z \approx 0.4$ for nine of the brighter objects with $I \lesssim 20.3$ mag, details of which are given elsewhere[15]. Results on all objects are summarized in Table 1. In January 1995, Lowenthal and Koo (personal communication) obtained redshifts with a long integration on the Keck telescope for another 6–8 galaxies down to $I \lesssim 22.5$ mag with measured redshifts up to $z \approx 0.7$. For three radio sources in the sample (13, 15, 19), as well as galaxies 14 and 22, HST light-profiles have been published[15]. They are dominated by an exponential disk. Of the remaining objects, galaxies 1, 6, 9, 10, 16, 18 and 24 are also dominated by exponential profiles. Galaxy 8 is too faint to be classified. Only galaxies 2 and 3 show a significant $r^{1/4}$ contribution to their light-profiles, and contain a clear bulge embedded in a disk. Hence, at least 67% of the microjansky sample consists of disk-dominated galaxies, generally with little or no colour gradients[15,19]. The observed range of exponential disk scale-lengths is $0.4'' \lesssim r_s \lesssim 2.7''$ with median $r_s \approx 0.8 \pm 0.2$ arcsec, somewhat larger than the median HST scale-length of 0.4 arcsec for faint field galaxies[16,20], indicating that our radio galaxies may be more luminous than ordinary field galaxies, as the absolute luminosity of galaxies is known to be proportional to their scale-length[18,20]. This is substantiated by the Hubble diagram for the few microjansky identifications with available redshifts: they have absolute luminosities $M_V = -22.2$ mag, comparable to those of sub-millijanksy and millijansky galaxies[28], but $\gtrsim 0.7$ mag brighter than typical field galaxies[20], so the microjansky population does not (yet) sample a large fraction of dwarf-like luminosities.

Two microjansky sources coincide with weak quasars, consistent with the fraction of active galactic nuclei (AGN) seen at brighter radio fluxes[8]. Both quasars are at the same redshift of $z = 2.561$ and are ~1.5 arcmin apart, which rules out a gravitational lens, but suggests that a group or cluster at $z \approx 2.56$ may be present in the field. The average $(V-I)$ colour of the microjansky radio galaxies in Table 1 is $1.5 \pm 0.7$ mag, similar to that of a much larger sample of HST field galaxies (with $V \approx 20$–24 mag)[16,20]. Five radio galaxies (6, 9, 18, 19 and 24) have colours as red as the upper envelope in the $(V-I)$ colour–magnitude diagram of HST field galaxies[16,18,20]. Four of these are located in pairs or groups, and may be post-starburst galaxies as seen in distant clusters[29]. The eight remaining galaxies in Table 1 have colours bluer than the red upper envelope of field galaxies[16,20]. Five of these also occur in pairs or groups. These are possibly galaxies with enhanced star-formation, induced by companions or interactions. The MMT spectra of the blue galaxies 3, 13, 15 and 19 have weak narrow emission lines (O II 3,727 Å and Hα of typical rest-frame equivalent width $W_\lambda \approx 20$–30 Å), suggesting star-formation.

Are the microjansky galaxies dominated by starbursts and/or by weak AGN? The flat high-frequency radio spectra[2] suggest possibly free–free or thermal dust-emission in extended disks[2], and/or compact synchrotron cores. The 60% of double or interacting identifications from the HST images, and the 67% of exponential disks among the HST identifications, suggest that the microjansky sources occur in a disk-dominated galaxy population that is undergoing interactions, with optical luminosities that generally exceed $L^*$. Combined with the fact that only 20–30% of microjansky sources are variable on timescales of years[2,13], but that >40% are extended radio sources[2] ($\gtrsim 5$ arcsec), our HST results suggest that the majority of the microjansky population is likely to be of a starburst or post-starburst nature, embedded in luminous disk galaxies and triggered by interactions or mergers, with only a minority of weak AGN. For $I \lesssim 20.5$ mag, these disk galaxies are seen out to a redshift $z \approx 0.4$, whereas at $I \approx 22.5$ mag, they are expected[2,20,28] to be at $z \lesssim 0.8$. Higher resolution VLA B-configuration and observations with the refurbished HST will help locate any weak AGN, as these may occur together with nuclear and/or global starburst in the microjansky radio sources, possibly triggered by the same dynamical disturbance. □

Received 2 March; accepted 2 May 1995.


1. Windhorst, R. A., Miley, G. K., Owen, F. N., Kron, R. G. & Koo, D. C. *Astrophys. J.* **289,** 494–513 (1985).
2. Windhorst, R. A., Fomalont, E. B., Partridge, R. B. & Lowenthal, J. D. *Astrophys. J.* **405,** 498–517 (1993).
3. Condon, J. J. *Astrophys. J.* **338,** 13–23 (1989).
4. Kellermann, K. I. & Wall, J. V. in *Observational Cosmology* (eds Hewitt, A., Burbidge, G. & Fang, L. Z.) 545–564 (IAU Symp. 124, Reidel, Dordrecht, 1987).
5. Fomalont, E. B., Windhorst, R. A., Kristian, J. A. & Kellermann, K. I. *Astr. J.* **102,** 1258–1277 (1991).
6. Fomalont, E. B., Partridge, R. B., Lowenthal, J. D. & Windhorst, R. A. *Astrophys. J.* **404,** 8–20 (1993).
7. Condon, J. J. *Astrophys. J.* **287,** 461–474 (1984).
8. Kron, R. G., Koo, D. C. & Windhorst, R. A. *Astr. Astrophys.* **146,** 38–58 (1985).
9. Weistrop, D., Wall, J. V., Fomalont, E. B. & Kellermann, K. I. *Astr. J.* **93,** 805–810 (1987).
10. Windhorst, R. A., Dressler, A. & Koo, D. C. in *Observational Cosmology* (eds Hewitt, A., Burbidge, G. & Fang, L. Z.) 573–576 (IAU Symp. 124, Reidel, Dordrecht, 1987).
11. Benn, C. R., Rowan-Robinson, M., McMahon, R. G., Broadhurst, T. J. & Lawrence, A. *Mon. Not. R. astr. Soc.* **263,** 98–122 (1993).
12. Thuan, T. X. & Condon, J. J. *Astrophys. J.* **322,** L9–L14 (1987).
13. Oort, M. J. A. & Windhorst, R. A. *Astr. Astrophys.* **145,** 405–424 (1985).
14. Donnelly, R. H., Partridge, R. B. & Windhorst, R. A. *Astrophys. J.* **321,** 94–112 (1987).
15. Windhorst, R. A. *et al. Astr. J.* **107,** 930–945 (1994).
16. Griffiths, R. E. *et al. Astrophys. J.* **437,** 67–82 (1994).
17. Windhorst, R. A., Mathis, D. F. & Keel, W. C. *Astrophys. J.* **400,** L1–L4 (1992).
18. Windhorst, R. A. *et al. Astrophys. J.* **435,** 577–598 (1994).
19. Keel, W. C. & Windhorst, R. A. *Astr. J.* **106,** 455–465 (1993).
20. Casertano, S. *et al. Astrophys. J.* (submitted).
21. Ratnatunga, K. U., Griffiths, R. E., Casertano, S., Neuschaefer, L. W. & Wyckoff, E. W. *Astr. J.* **108,** 2362–2372 (1994).
22. Condon, J. J. *A. Rev. Astr. Astrophys.* **30,** 575–612 (1992).
23. Windhorst, R. A., Kron, R. G. & Koo, D. C. *Astr. Astrophys. Suppl. Ser.* **58,** 39–87 (1984).
24. Mitchell, K. *et al. Publ. astr. Soc. Pacif.* **93,** 647–654 (1981).
25. Ostriker, J. P. & Heisler, J. *Astrophys. J.* **278,** 1–10 (1984).
26. Burkey, J. M., Keel, W. C., Windhorst, R. A. & Franklin, B. E. *Astrophys. J.* **429,** L013–L017 (1994).
27. Griffiths, R. E. *et al. Astrophys. J.* **435,** L019–L022 (1994).
28. Windhorst, R. A., Mathis, D. F. & Neuschaefer, L. W. in *Evolution of the Universe of Galaxies* (ed. Kron, R. G.) 389–403 (ASP Conf. Ser. Vol. 10, Bookcrafters, Provo, UT, 1990).
29. Dressler, A. & Gunn, J. E. *Astrophys. J.* **270,** 7–19 (1983).
30. Patnaik, A. R., Browne, I. W. A., Wilkinson, P. N. & Wrobel, J. M. *Mon. Not. R. astr. Soc.* **254,** 655–676 (1992).


ACKNOWLEDGEMENTS. Some observations reported here were made by The NASA/ESA Hubble Space Telescope, obtained at the Space Telescope Science Institute (STScI), which is operated by the Association of Universities for Research in Astronomy, Inc., under contract to NASA. Some optical observations were obtained at the Multiple Mirror Telescope Observatory, a joint facility of the University of Arizona and the Smithsonian Institution. Some observations were obtained at the National Radio Astronomy Observatory, which is operated by Associated Universities Inc., under cooperative agreement with the US NSF. We thank the VLA and STScI staff for their continuous help, and E. Wyckoff for help with the WF/PC image stacking. This work was supported by two NASA/HST grants from STScI, and by the US NSF.

# Extreme elongation of asteroid 1620 Geographos from radar images

**S. J. Ostro*, K. D. Rosema*, R. S. Hudson†, R. F. Jurgens*, J. D. Giorgini*, R. Winkler*, D. K. Yeomans*, D. Choate*, R. Rose*, M. A. Slade*, S. D. Howard* & D. L. Mitchell***

* Jet Propulsion Laboratory, California Institute of Technology, Pasadena, California 91109-8099, USA
† School of Electrical Engineering and Computer Science, Washington State University, Pullman, Washington 99164-2752, USA

**MOST small asteroids are thought to result from catastrophic collisions[1], and their shapes can provide insight into their origin and collisional evolution. Two main-belt asteroids have been successfully imaged by spacecraft[2,3], but such images have yet to be obtained for asteroids that cross Earth's orbit. Earth-crossing asteroids are generally too small to be resolved by optical telescopes, and shape constraints derived from optical lightcurves are subject to large systematic biases[4]. Ground-based radar observations, on the other hand, have proved successful in resolving the**

TABLE 1 Observation parameters

| Date | Runs | UTC interval | Phase interval |
|---|---|---|---|
| 30 Aug. | 3 | 05:15–05:20 | 310°–315° |
| | 43 | 05:23–07:07 | 320°–64° |
| | 50 | 07:13–09:02 | 86°–211° |
| | 27 | 09:07–10:01 | 218°–279° |
| 31 Aug. | 21 | 03:39–04:30 | 59°–120° |
| | 52 | 05:43–07:28 | 202°–322° |
| | 54 | 07:38–09:27 | 335°–99° |

Columns give date in August 1994, the number of runs, the UTC time interval, and the rotation-phase interval for each sequence of 0.5-μs imaging runs. Breaks between sequences were either caused by equipment problems or introduced to allow data transfer between acquisition and analysis computers. Geographos's topocentric right ascension, declination and distance near the middle of the observations on 30 and 31 August were (321.6° and 321.7°, respectively), (−23° and −18°) and (0.048 and 0.053 AU). All observations employed transmission of a circularly polarized signal and reception of echoes in the orthogonal circular polarization. We used a repetitive, binary-phase-coded waveform[38] with a 127-element code that provided 127 'range bins', each with a time resolution, 0.5 μs, equal to the temporal extent of each code element. Application of a 64-point fast Fourier transform to successive, decoded voltage samples from a single range bin sorted those echoes into 64 frequency bins[39]. Each delay-Doppler image was constructed by repeating this process for each range bin.

**shapes of some small asteroids[5–9]. We describe here radar measurements of the Earth-crossing asteroid 1620 Geographos during its recent close encounter with the Earth. We have determined the silhouette of Geographos along its rotation axis, and confirm earlier lightcurve-based conjectures[10] that this object has a very unusual shape. The silhouette is irregular, non-convex and has an aspect ratio of 2.76 ± 0.21, establishing it as the most elongated Solar System object yet imaged. The unusual nature of the shape is underscored by laboratory fragmentation experiments[11,12], in which the average aspect ratio of fragments is 1.4, with fewer than 1% as elongated as Geographos.**

The Earth-crossing Apollo asteroid 1620 Geographos was discovered at Palomar Observatory on 14 September 1951, by A. G. Wilson and R. Minkowski. Geographos approached to within 0.061 AU of Earth on 26 August 1969, and extensive photometric and polarimetric observations by Dunlap[10] during January, August, September and October of that year yielded lightcurves whose enormous brightness oscillations ($B_{max}/B_{min}$ as large as 6.5) exceeded those observed for any other asteroid, a distinction that still holds. The 1969 results prompted speculations about a "cigar-shaped" object and inspired a painting by *National Geographic* artist D. Meltzer (p. 175 of ref. 13) that also forms the frontispiece for the first modern scientific book on asteroids[14].

In August 1994, Geographos passed within 0.034 AU of Earth, its closest approach for at least the next two centuries. The asteroid entered the declination window of the Goldstone radar on 28 August and we observed it daily for one week, obtaining hundreds of images. Here we present the first results from our highest-resolution observations.

Each of our images shows the distribution of echo power in time delay (range) and Doppler frequency (radial velocity). Contours of constant delay are defined by planes normal to the line of sight, and for a rotating rigid body, contours of constant frequency are defined by planes parallel to both the line of sight and the target's apparent spin vector. Thus, each image cuts the target into cells that are parallel to the apparent spin vector's plane-of-sky projection[15]. Constraints on Geographos's pole direction from optical lightcurves[10,16] indicate that Goldstone was within 10° of the asteroid's equatorial plane throughout the radar observations, so the delay-Doppler cells remain nearly normal to the asteroid's equatorial plane at all rotation phases. Because each cell can capture echoes from surface regions north and south of the equator, an image is a 'double exposure' that contains an intrinsic north/south ambiguity. However, sums of co-registered images over a sufficient range of phases can unambiguously define the asteroid's pole-on silhouette, that is, the outline of the object when viewed from along the pole.

Our highest-resolution observations consisted of 250 runs on 30–31 August (Table 1). In each run, Goldstone's 70-m antenna (DSS 14) transmitted a 450-kW signal for ~50 s and then received echoes for a somewhat shorter duration. The combination of the transmitted waveform's modulation and our real-time processing of received signals provided a time resolution of 0.5 μs (75 m in range) and a frequency resolution of 1.64 Hz (2.9 cm $s^{-1}$ in radial velocity). The length equivalent (87 m) of the frequency resolution and our rotation-phase assignments were calculated from a topocentric ephemeris and comprehensive, lightcurve-based estimates (P. Magnusson, personal communication) of the spin period (5.22332784 ± 0.00000096 h) and the pole direction (ecliptic longitude, latitude is 55° ± 5°,

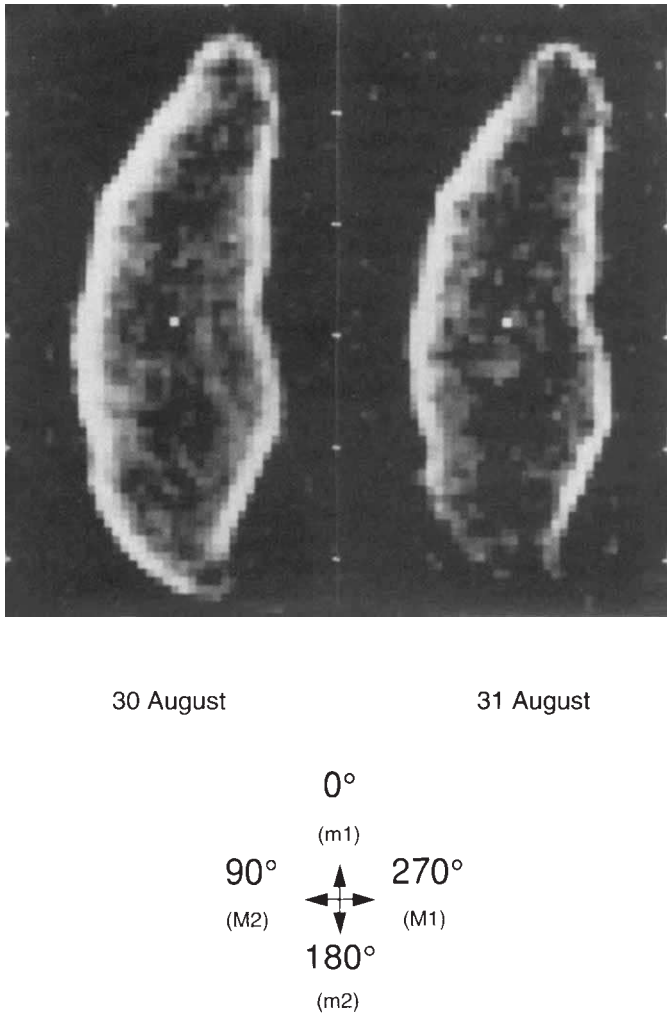


FIG. 1 Estimates of Geographos's pole-on silhouette from co-registration and summation of all 0.5-μs images obtained on 30 and 31 August 1994. The salient information in this image is the periphery of the echo distribution; the grey-scale is arbitrary and no meaning is attached to brightness variations inside the silhouette. The tick marks on the borders are 1 km apart. The central white pixel locates the asteroid's centre of mass. Our rotation-phase origin (0° in the diagram below the images) corresponds to the asteroid's end-on orientation near primary (dimmest) lightcurve minimum m1, which follows primary (brightest) lightcurve maximum M1. Geographos's lightcurves show extrema in the chronological order m1, M2, m2, M1, corresponding to phases near 0°, 90°, 180° and 270°. Arrows indicate the direction to the radar at each of those phases.

$-45° \pm 5°$); relative errors in our phase assignments are thought to be very small compared to the ~0.6° phase resolution of each run.

The extremely high noise level in images from individual runs is reduced by an order of magnitude when all the runs from a given date are summed. Our precise knowledge of the spin period makes rotational co-registration of images straightforward. Of more concern is "translational smearing" caused by imperfect knowledge of the delay-Doppler location of the centre of mass from image to image. Our prediction ephemerides were accurate enough to prevent perceptible smearing over timescales of the order of 10 min, but much longer summations require an *a posteriori* ephemeris that is at least two orders of magnitude more accurate. Preliminary application of several analysis methods[9,17] to low-resolution data from 28 August to 2 September has produced an ephemeris for which the centre-of-mass trajectory during 30–31 August is believed to contain uncertainties that degrade the data's intrinsic resolution by no more than several tens of per cent on each day.

Figure 1 shows estimates of Geographos's pole-on silhouette from co-registration and summation of single-run images. Although the echoes were stronger and the phase coverage was better on 30 August, the two estimates are in excellent agreement. Our estimates of the silhouette's extreme breadths (that is, the extreme dimensions of its convex envelope) are $5.11 \pm 0.15$ km and $1.85 \pm 0.15$ km; the stated uncertainties are subjective standard errors. Our estimate of the asteroid's elongation (that is, the ratio of the silhouette's extreme breadths) is $\beta = 2.76 \pm 0.21$; we have assumed a cross-correlation coefficient[18] of 0.5 between uncertainties in the breadth estimates, because they suffer similar biases from errors in the *a posteriori* ephemeris. These results show that lightcurve-based predictions about Geographos's elongation were accurate. For example, Dunlap's[10] 'best fitting model (a cylinder with hemispherical ends) had a length to width ratio of 2.7, which results in Geographos being $1.50 \pm 0.15$ km wide and $4.0 \pm 0.5$ km long', and Kwiatkowski[16] reported an ellipsoidal model with $\beta = 2.5 \pm 0.3$. The most exhaustive study of Geographos lightcurves to date yields an ellipsoidal model with $\beta = 2.58 \pm 0.16$ (ref. 19). Our results also support the general conclusion (resulting from the Galileo spacecraft flybys of the much larger, main-belt asteroids 951 Gaspra and 243 Ida) that shape models based on well determined lightcurves are reliable predictors of those objects' elongations[2,3,20,21].

How rare is Geographos's elongation among the Earth-crossing asteroids (ECAs) and main-belt asteroids (MBAs) of similar size? Optical lightcurves are available for dozens of ECAs and small MBAs, and a lightcurve's peak-to-valley amplitude, that is, the ratio of the maximum and minimum brightnesses $B_{max}/B_{min}$, is often taken as a crude indicator of elongation despite the potentially strong dependence of $B_{max}/B_{min}$ on viewing/illumination geometry[4]. Binzel *et al.*[22] noted that whereas amplitudes taken at face value implied mean elongations of ~1.6 for 32 ECAs and ~1.3 for 32 small MBAs, mean elongations between 1.2 and 1.3 were inferred for both groups if 'global' corrections were applied to the amplitudes to compensate for primary sources of bias. Radar delay-Doppler and Doppler-only images have yielded direct determinations of $\beta$ for the Mars-crossing asteroid 433 Eros[23] ($\beta \approx 2.1$) and about a dozen ECAs, including 1627 Ivar[6] ($\beta \approx 2.1$), and 4769 Castalia[9] ($\beta \approx 1.6$). Those asteroids, as well as Gaspra[24] ($\beta \approx 1.7$), Ida[3,25] ($2.23 \leqslant \beta \leqslant 2.39$), and all other Solar System objects for which $\beta$ has been measured from optical images[26,27], are less elongated than Geographos.

What can be said about the detailed sequence of collisional events that produced Geographos's remarkable elongation? Current understanding of collisional processes rests largely on hypervelocity fragmentation experiments and theoretical scaling laws[11,12,28]. Laboratory experiments have involved a wide range of impact velocities and target/projectile materials[29–31], including weakly bonded aggregates of stronger constituent particles[32]. Mean fragment elongations from experiments reported so far are typically ~1.4, with fewer than 1% as elongated as Geographos. For experiments that used open-air detonation of spherical targets by explosive contact charges[33], mean fragment elongations are ~1.7, with several per cent more elongated than Geographos. Breakage of fragments against chamber walls in experiments not carried out in the open may or may not bias results toward smaller elongations. On the other hand, small asteroids are thought to be the product of several generations of disruptive collisions[1], so one might argue that experiments involving secondary fragmentation against chamber walls provide the more relevant results. Capaccioni *et al.*[34] noted a tendency for fragments generated farther from the impact point to become larger and possibly more irregular in shape, and Paolicchi *et al.*[35] suggested that elongated fragments may be more likely if the collision-induced velocity field is highly asymmetric, but other clues about how elongated fragments might form are lacking. Furthermore, the degree to which laboratory results can accurately be extrapolated to asteroidal scales may be rather limited[28].

Apart from its gross dimensions, one of the more interesting attributes of Geographos's silhouette is the disparity between the contours of its two long sides. The middle of the M1 side (Fig. 1) contains a prominent indentation, but the entire length of the opposite (M2) side is nearly convex at the 100-m scale. To our eyes, the silhouette's shape seems more suggestive of a monolithic fragment derived from a disruptive collision than a compound, multi-component product of a constructive collision. However, our data hardly rule out the latter possibility. Moreover, if Geographos were an agglomeration of disparate fragments[36], clues about this configuration might not be evident from the silhouette. A three-dimensional model of Geographos could prove more informative, but due to the equatorial view of our observations, inversion of the images using the technique applied successfully to Castalia[9] cannot produce a unique three-dimensional model of Geographos. Inclusion of lightcurves in the inversion may provide the additional geometrical information required for such a reconstruction[37]. □

Received 24 March; accepted 17 May 1995.


1. Farinella, P., Paolicchi, P. & Zappalà, V. *Icarus* **52,** 409–433 (1982).
2. Belton, M. J. S. *et al. Science* **257,** 1647–1652 (1992).
3. Belton, M. J. S. *et al. Science* **265,** 1543–1547 (1994).
4. Zappalà, V., Cellino, A., Barucci, M. A., Fulchignoni, M. & Lupishko, D. F. *Astr. Astrophys.* **231,** 548–560 (1990).
5. Ostro, S. J., Campbell, D. B. & Shapiro, I. I. *Astr. J.* **88,** 565–576 (1983).
6. Ostro, S. J. *et al. Astr. J.* **99,** 2012–2018 (1990).
7. Ostro, S. J. *et al. Science* **252,** 1399–1404 (1991).
8. Ostro, S. J. *et al. Science* **248,** 1523–1528 (1990).
9. Hudson, R. S. & Ostro, S. J. *Science* **263,** 940–943 (1994).
10. Dunlap, J. L. *Astr. J.* **79,** 324–332 (1974).
11. Fujiwara, A. *et al.* in *Asteroids II* (eds Binzel, R. P., Gehrels, T. & Matthews, M. S.) 240–265 (Univ. Arizona Press, Tucson, 1989).
12. Nakamura, A. *Laboratory Studies on the Velocity of Fragments from Impact Disruption* (ISAS Rep. 651, Inst. of Space and Astronautical Science, Yoshinodai Sagamihara, Kanagawa, Japan, 1993).
13. Weaver, K. F. *Nat. Geogr. Mag.* **138**(2), 147–193 (1970).
14. Gehrels, T. (ed.) *Physical Studies of Minor Planets* (NASA SP-267, US Govt Printing Office, Washington DC, 1971).
15. Hudson, R. S. *Remote Sensing Rev.* **8,** 195–203 (1993).
16. Kwiatkowski, T. *Astr. Astrophys.* **294,** 274–277 (1995).
17. Ostro, S. J., Connelly, R. & Belkora, L. *Icarus* **73,** 15–24 (1988).
18. Finney, D. J. *Statistical Method in Biological Assay* 2nd edn (Hafner, New York, 1964).
19. Magnusson, P. *Icarus* (submitted).
20. Magnusson, P. *et al. Icarus* **97,** 124–129 (1992).
21. Binzel, R. P. *et al. Icarus* **105,** 310–325 (1993).
22. Binzel, R. P., Xu, S., Bus, S. J. & Bowell, E. *Science* **257,** 779–782 (1992).
23. Ostro, S. J., Rosema, K. D. & Jurgens, R. F. *Icarus* **84,** 334–351 (1990).
24. Thomas, P. C. *et al. Icarus* **107,** 23–36 (1993).
25. Thomas, P. *et al.* (abstr.) *Bull. Am. astr. Soc.* **26,** 1155 (1994).
26. Burns, J. A. in *Satellites* (ed. Burns, J. A.) 1–38 (Univ. Arizona Press, Tucson, 1986).
27. Rahe, J., Vanysek, V. & Weissman, P. R. in *Hazards Due to Comets and Asteroids* (ed. Gehrels, T.) 597–634 (Univ. Arizona Press, Tucson, 1994).
28. Housen, K. R. & Holsapple, K. A. *Icarus* **84,** 226–253 (1990).
29. Gault, D. E. & Wedekind, J. A. *J. geophys. Res.* **74,** 6780–6794 (1969).
30. Cerroni, P. *Memorie Soc. astr. ital.* **57,** 13–45 (1986).
31. Fujiwara, A. *Memorie Soc. astr. ital.* **57,**47–64 (1986).
32. Ryan, E. V., Hartmann, W. K. & Davis, D. R. *Icarus* **94,** 283–298 (1991).
33. Giblin, I. *et al. Icarus* **110,** 203–224 (1994).
34. Capaccioni, F. *et al. Icarus* **66,** 487–514 (1986).

35. Paolicchi, P., Cellino, A., Farinella, P. & Zappalà, V. *Icarus* **77,** 187–212 (1989).
36. Bottke, W. F. Jr & Melosh, H.J. *Lunar Planet. Sci. Conf. Abstr.* **26,** 153–154 (1995).
37. Hudson, R. S., Ostro, S. J. & Harris, A. W. (abstr.) *Bull. Am. astro. Soc.* **26,** 1173 (1994).
38. Ostro, S. J. *Rev. Mod. Phys.* **65,** 1235–1279 (1993).
39. Priest, P. *Goldstone Solar System Radar Capability and Performance* (JPL Internal Rep. 1740-4, Jet Propulsion Laboratory, Pasadena, 1993).

ACKNOWLEDGEMENTS. We thank the Goldstone technical staff for their support of these observations. Part of this research was conducted at the Jet Propulsion Laboratory, California Institute of Technology, under contract with NASA.

# Ice in the 1994 Rabaul eruption cloud: implications for volcano hazard and atmospheric effects

**W. I. Rose*, D. J. Delene*, D. J. Schneider*, G. J. S. Bluth*, A. J. Krueger†, I. Sprod†, C. McKee‡, H. L. Davies§ & G. G. J. Ernst‖**

* Geological Engineering and Sciences, Michigan Technological University, Houghton, Michigan 49931, USA
† NASA Goddard Space Flight Center, Greenbelt, Maryland 20771, USA
‡ Rabaul Volcano Observatory, PO Box 386, Rabaul, Papua New Guinea
§ University of Papua New Guinea, PO Box 414, University, Papua New Guinea
‖ Department of Geology, University of Bristol, Bristol BS8 1RJ, UK

**VOLCANIC clouds are an important natural hazard to aircraft[1], and host chemical reactions that interest both volcanologists[2,3] and atmospheric scientists[4–6]. Ice has been suggested as a possible component of eruption clouds[7], but there has been no direct evidence for its presence. Here we report the detection, using a satellite-borne infrared sensor, of $\gtrsim$2 million tonnes of ice in the cloud produced by the September 1994 eruption of Rabaul volcano, in Papua New Guinea. The cloud also contained relatively low levels of sulphur dioxide (80 ± 50 kilotonnes), compared with other stratospheric eruption clouds. The unusual aspects of this cloud may be related to the entry of sea water into the volcanic vent, and its participation in the eruption column. Past eruptions that occurred in similar (coastal) settings, such as those of Krakatau and Santorini, might have had less effect on the atmosphere than their volume alone would suggest, because the presence of ice may decrease the residence time of ash and sulphur in the atmosphere. In addition, the ability of ice to mask the characteristic spectral signature of volcanic ash will increase the difficulty of designing airborne ash detection systems for aviation safety.**

The 1994 Rabaul eruption began on 19 September with nearly simultaneous outbursts from two vents (Tavurvur, 06:06 local time; Vulcan, 07:17 local time) on opposite sides of the caldera (Fig. 1 inset). The Vulcan eruption was more powerful, with column heights estimated at 20 km, whereas Tavurvur's column reached a maximum height[8] of 6 km. Some of the ash fallout was very wet, and a 'rain of mud' occurred in some areas around Rabaul. Sea water had access to the main active vent low on the northeastern flank of Vulcan, and salty rainfalls took place in a wide arc north and northwest of Vulcan during 19 and 20 September[8]. The tephra fall deposits resulting from Vulcan's eruptions contained ubiquitous sea-salt deposits.

The advanced very-high-resolution radiometer (AVHRR) detector aboard the NOAA 12 polar-orbiting satellite was used for mapping the volcanic cloud and determining the composition, size and mass of its particles based on data collected on 19 September at 09:00 UT (19:00 local time) and again at 21:50 UT (20 September, 07:50 local time). The dispersal pattern shown by the Rabaul cloud was marked by a broad fan shape (Fig. 2), probably caused in part by upper-level winds; many volcanic clouds, particularly at middle and high latitudes, are more directionally focused[9] than this.

Multi-wavelength AVHRR images have two thermal infrared channels (band 4, $\lambda = 10.3$–$11.3$ μm; band 5, $\lambda = 11.5$–$12.5$ μm) which can be used for estimation of the sizes, masses and some compositional characteristics of particles in the cloud[10]. Silicate ash and concentrated sulphuric acid aerosol particles in transparent drifting volcanic clouds have distinctive negative band 4 − band 5 apparent temperature differences[11–14]. Figure 3*a* shows a plot of band 4 − band 5 temperature differences versus band 4 temperatures for the individual pixels comprising Fig. 2. For comparison, Fig. 3*b* shows a similar plot for the volcanic cloud arising from the Klyuchevskoi eruption. The Klyuchevskoi cloud is representative of many volcanic clouds which have negative band 4 − band 5 temperature differences. The positive band 4 − 5 temperature difference exhibited by the Rabaul cloud is unique among a dozen eruptions that we have studied with this method[13]; the volcanic cloud shows no silicate or sulphate signal. The observed temperature differences were compared with simulated temperature differences calculated using refractive indices for ice (Fig. 3*a*), which demonstrates that Rabaul's cloud had the spectral characteristics of spherical ice particles with effective radii of 9–40 μm. (In reality, the cloud will have contained particles with radii outside this range.) Note that the temperature of the opaque portion of the Rabaul eruption cloud is ~190 K (−83 °C), corresponding to the inferred tropopause temperature from the radiosonde data.

We compare Rabaul to the Klyuchevskoi eruption because the Klyuchevskoi cloud is much more like other volcanic clouds we have studied, was similar in scale to Rabaul, although smaller, and was examined by the same AVHRR detector only 12 days after it observed Rabaul's cloud. The Klyuchevskoi cloud contained more $SO_2$ than Rabaul's, although little ice, and was driven by stronger (40–65 m $s^{-1}$) northwesterly winds at an altitude of 12–13 km. The Klyuchevskoi cloud exhibited no significant wind shear (P. Newman, personal communication) and a focused dispersal pattern which extended in an elongated plume across the northern Pacific. The effective radii of the ice particles in the Rabaul cloud are larger than the particle sites that we have observed in volcanic clouds with silicate signals, such as Klyuchevskoi. The effective particle radius inferred for the Klyuchevskoi eruption cloud was in the range 1–12 μm.

Using the methods of Wen and Rose[10], we computed the total masses of ice in the transparent (optical depth < 4) parts of the Rabaul cloud and found a mass of 2–3 megatonnes (Mt). This mass is ten times the mass of silicates calculated for the Klyuchevskoi cloud (0.1–0.3 Mt). The particle mass contained in the transparent part of a volcanic cloud during an eruption is a small fraction (< 1%) of the total[10], as most of the mass is in the opaque near-vent portion of the cloud. The opaque por-

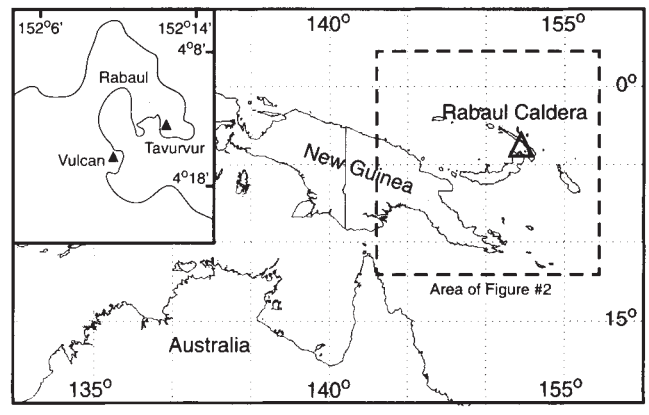


FIG. 1 Location maps for Rabaul caldera.